J Mater Sci (2011) 46:468–478
DOI 10.1007/s10853-010-4931-4

Effect of $BaSO_4$ on the interfacial phenomena of high-alumina refractories with Al-alloy

Pramod Koshy · Sushil Gupta · Phil Edwards · Veena Sahajwalla

Received: 10 August 2010 / Accepted: 15 September 2010 / Published online: 28 September 2010

Abstract The performance of high-alumina refractories used for aluminium casting significantly impacts the efficiency of metal production. The interfacial reactions with Al-alloys cause corundum and magnesium spinel deposition on the refractory surface, leading to refractory degradation. An experimental study was conducted to investigate the influence of varying barium sulphate ($BaSO_4$) concentrations in a high-alumina refractory on its interfacial reactions with molten Al-alloy in a horizontal tube furnace at 1523 K (1250 °C) under inert conditions. This study showed that the Al-alloy reactions with pure $BaSO_4$ would form barium aluminates at the interface. However, in the Al-alloy/refractory system, the interfacial behaviour was strongly influenced by the relative amount of $BaSO_4$, such that up to 5 wt%, the extent of alloy penetration into the refractory increased with increasing $BaSO_4$ contents. Electron-probe micro-analyser and X-ray diffraction studies indicated that the composition of the interface for these refractories was augmented with barium silicates and diminishing anorthite phases. In the presence of 10 wt% $BaSO_4$, the extent of metal penetration into the refractory decreased, whilst for 20% $BaSO_4$, the penetration was higher; these results were attributed to the interfacial presence of celsian ($BaAl_2Si_2O_8$) and unreacted barium sulphates, respectively. This study suggests that maximising the celsian formation at the interface is critical for optimising the $BaSO_4$ concentration for improving the refractory's performance for Al-casting.

P. Koshy (✉) · S. Gupta · V. Sahajwalla
Centre for Sustainable Materials Research and Technology, School of Materials Science & Engineering, University of New South Wales, Sydney, NSW 2052, Australia
e-mail: koshy@unsw.edu.au

P. Edwards
Shinagawa Refractories Australasia Pty Ltd, Unanderra, NSW 2526, Australia

Introduction

Aluminium manufacturing is an energy-intensive process where a quarter of the energy consumed is used for melting and holding furnace operations [1]. In aluminium cast houses, the behaviour of the refractory materials lining the treatment furnaces has a major impact on the efficiency of hot metal processing and the quality of hot metal produced [2]. The melting furnaces usually operate over the temperature range 973–1673 K (700–1400 °C) [3, 4], and their refractory linings undergo corrosive failure due to molten metal reactions [4, 5]. These reactions lead to the formation of an interfacial buildup on the refractory surface, which reduces the efficiency and service life of the refractory lining [6]. The formation of these deposits is associated with stress fractures, whilst their removal by scraping can damage the lining.

High-alumina refractories are now commonly used in casting furnaces [7, 8]. Previous studies have analysed the interfacial behaviour of pure Al/Al_2O_3 systems for metal–ceramic composites [9–14]. However, this is considerably different to Al-casting refractories due the different forms and contents of silica present in the high-alumina refractory as well as the different alloying constituents (Mg and Zn) present in the metal. Furthermore, the complexity of the interfacial behaviour in these systems is enhanced greatly by the presence of non-wetting agents, making it difficult to interpret the refractory behaviour based on the findings from the pure Al/Al_2O_3 system alone.

Refractory corrosion by molten metals/alloys begins with the initiation of wetting reactions at the interface and

is subsequently followed by metal penetration and formation of secondary phases such as corundum or spinel [15–19]. In addition to the thick buildup on the refractory walls formed by the secondary phases, the alloy also gets contaminated through the refractory reactions. Several factors affect the refractory reactions with Al-alloys. The effect of physical properties (such as the porosity, surface roughness and particle sizes) as well as the processing conditions on the interfacial behaviour of Al/Al_2O_3 systems have been well documented [10–18, 20–23]. However, there is limited understanding of the effect of non-wetting additives (such as barium sulphate ($BaSO_4$) on the interfacial reactions of the Al-alloy/high-alumina refractory system, and there is also an ambiguity about the mechanisms involved [24]. Silica reduction by Al-alloys is one of the major reactions that contributes to corundum buildup and metal contamination [5, 22] (Eq. 1).

$$3SiO_{2(\text{refractory})} + 4Al_{(\text{metal})} \rightarrow 2Al_2O_{3(\text{corundumdeposit})} + 3Si_{(\text{metal})} \quad (1)$$

Silica is often added to improve the thermo-mechanical properties of refractories [24–26] and can occur as free quartz, mullite and microsilica. Even though mullite is the most thermodynamically stable phase in the Al_2O_3–SiO_2 phase diagram, it can also be reduced by molten Al similar to silica, though at a slower rate [22].

Often, non-wetting additives such as barium sulphate ($BaSO_4$), calcium fluoride (CaF_2) and aluminium fluoride (AlF_3) [23–29] are added to the refractories to improve their corrosion resistance to molten alloys; the nature and quantity of the agents is believed to be influenced by the composition of the refractory [23]. However, there are uncertainties with regard to both their application in high-alumina refractories and the relevant mechanisms [30]. $BaSO_4$ is believed to form barium aluminosilicates ($BaAl_2Si_2O_8$), and this decreases the free silica available for reduction [24, 27]. However, the effect of $BaSO_4$ in aluminosilicate refractories (>25 wt% SiO_2) has been reported to significantly change at temperatures >1323 K (1050 °C) such that the alloy penetration increased. This was attributed to either the structural transformation of the barium aluminosilicate phase (from hexacelsian to celsian ($BaAl_2Si_2O_8$)) [24] or due to metakaolin decomposition to mullite and free silica [31]. Hexacelsian is only stable close to 1873 K (1600 °C), though it can form as a metastable phase during the transformation of celsian ($BaAl_2Si_2O_8$), and is often retained at lower temperatures owing to the slow kinetics of celsian formation [32]. Even though some studies suggested that celsian is more reactive to the alloy than hexacelsian [24], others have shown that the presence of celsian in the refractory helps to resist molten aluminium reactions and subsequent penetration [28].

This article presents an investigation of the interfacial behaviour of high-alumina refractories with Al-alloy 7075 in the presence of $BaSO_4$ at 1523 K (1250 °C) in an inert atmosphere in order to clarify the mechanisms of the interfacial reactions. Electron Probe Micro Analysis (EPMA) and X-ray diffraction (XRD) data are presented to highlight the strong influence of the concentration of $BaSO_4$ in the alloy–refractory reactions at the interface. The observed interfacial phases were found to be consistent with thermodynamic predictions.

Experimental

Barium sulphate ($BaSO_4$, ~99% purity) and industrial grade high-alumina refractory samples were obtained from Shinagawa Refractories Australasia Pty Ltd. Table 1 gives the composition of the base refractory. Substrates were made by blending 0, 1, 3, 5, 10 and 20 wt% $BaSO_4$ to the refractory, and the samples prepared are referred to as BR0, BR1, BR3, BR5, BR10 and BR20, respectively. Chemical grade alumina (Aldrich, Steinheim, Germany) and silica (Sigma, St. Louis, MO) with 99% purity were also used in this study.

The substrates were prepared by compacting 2.5 g refractory powder under 7 tonne hydraulic load for 1 min. The substrate after compaction had a diameter of 20 mm and a thickness of 3–4 mm. The compacted substrates were heated at 1523 K (1250 °C) for 2 h in order to minimise the effect of gas evolution from the substrates. A narrow size range (<50 μm) was used to minimise the effect of particle size on the surface properties. Calcium aluminate binder present in the refractory mix ensured complete sintering of the substrates during the heat treatment stage.

Al-alloy 7075 was used due to its aggressive nature of reactions with the refractory (Table 2). The alloy was freshly cut in the form of cubes (~0.2 g) and then cleaned ultrasonically in acetone for 15 min. A horizontal furnace (Fig. 1), frequently used in interfacial studies [33–37], was used here as well. Before starting the experiments, the

Table 1 Chemical composition of the refractory without additive (BR0)

Phases	Al_2O_3	SiO_2	Fe_2O_3	TiO_2	CaO
Approx wt%	83	11	1	2	3

Table 2 Chemical composition of Al-alloy 7075

Element	Al	Zn	Mg	Cu	Fe, Si
wt%	91	5	2.4	1	<0.2

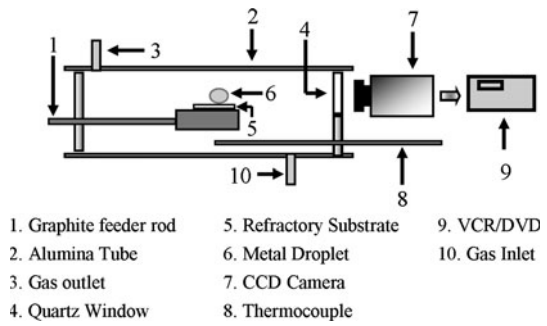

Fig. 1 Schematic of the sessile drop experimental setup used for conducting the interfacial studies

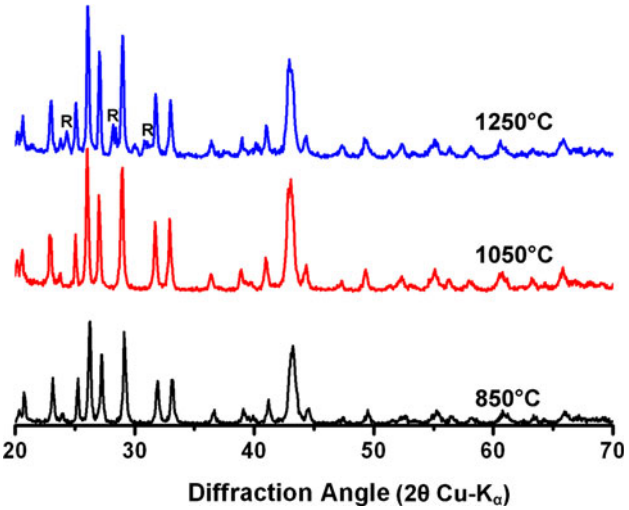

Fig. 2 XRD patterns showing the thermal stability of $BaSO_4$ in the absence of Al-alloy after heat treatment for 2 h at different temperatures (R-Structurally different Barium sulphate, all other peaks are original $BaSO_4$)

furnace was purged with high purity argon gas (99.999% purity, <1 ppm O_2) at 2 L/min for 30 min. The alloy specimen was then kept on the preheated refractory substrate which was then located on a graphite sample holder. This assembly was then inserted into the furnace hot zone in the presence of purging argon. All the tests were conducted at 1523 K (1250 °C) for 2 h.

Due to the very low solubility limit of oxygen in aluminium, extremely low equilibrium partial pressure of oxygen (10^{-44} Pa) is required to avoid complete oxidation [38, 39]; this is practically difficult to achieve under normal experimental conditions. At our test temperature of 1523 K (1250 °C), the oxidation effect was insignificant on the interfacial reactions as the oxide layer is believed to break up above 1273 K (1000 °C) [40]. Moreover, transient phases were easier to identify due to high intensity of reactions at these temperatures [33, 34]. A spherical and symmetrical droplet was formed after melting of the irregular alloy piece within 2–3 min after the start of the experiment, as was also observed in previous studies [30, 33, 34].

Siemens D5000 X-ray diffractometer using Cu Kα radiation (30 kV, 30 mA) was used to confirm the presence of crystalline phases using a finely crushed powder of the refractory specimens. The scattering intensity data were collected over an angular range 15–90° at the rate of one degree/min and a step size (resolution) of 0.05°.

The metal-refractory specimen was embedded in epoxy resin, and the interface was polished to a 0.5 μm finish. Elemental distribution at the metal–refractory interface was examined using EPMA (Cameca SX50). The EPMA was run using WDS (Wavelength Dispersive Spectroscopy) mode at 15 kV and 20 nA current. A symmetrical grid size (512 × 512 μm or 1024 × 1024 μm) was selected to map the elemental concentrations of Al, Mg, Si, O, Ca, Ba and S in various regions of the metal–refractory interface. SEM (Scanning Electron Microscopy, Hitachi S-3400X) was also used to analyse the interfacial microstructure of the polished samples. BSE (Back Scattered Electron) images were taken of the interfacial regions, whilst the porosity of the samples was estimated from the microstructural images using Image-J processing software. The polished samples were carbon-coated before EPMA or SEM analysis to improve the conductivity of the substrates.

Results and discussion

Thermal decomposition of $BaSO_4$

Thermodynamically, barium sulphate is believed to not decompose to BaO until 1823 K (1550 °C) [41–43]. However, in our conditions, it appears to have decomposed even at 1523 K (1250 °C) as seen in a previous study [30]. To understand the decomposition behaviour as well as the reactions of $BaSO_4$ with the refractory constituents, different sets of experiments were conducted. Pure barium sulphate samples were heat-treated at temperatures varying from 1123 to 1523 K (850–1250 °C) in the furnace under argon atmosphere, and then the phase transformations in the sample were analysed using X-ray diffraction (Fig. 2). Figure 2 shows that the major peak positions and intensities of $BaSO_4$ did not change after heat treatment for 2 h at any of the temperatures [1123 K (850 °C), 1323 K (1050 °C) and 1523 K (1250 °C)]. However, careful examination of the XRD pattern at 1523 K (1250 °C) shows a few additional minor peaks which were attributed to the modification of lattice parameters (analysed using Philips Xpert High Score). This suggests that $BaSO_4$ did not change its structure up to 1323 K (1050 °C), whilst at 1523 K (1250 °C), minor structural transformations occurred in the material which

could be related to the loss of sulphur-containing species through decomposition reactions. Weight loss calculations further revealed a change of less than 5% in the samples heated at 1523 K (1250 °C), which could be due to the decomposition reactions. The weight loss in the samples heated at the lower temperatures was less than 1%.

Thermal decomposition of $BaSO_4$ with silica and alumina

Figure 3 shows the XRD patterns of the $BaSO_4$ mixture (wt%) with Al_2O_3 (1:1) and SiO_2 (1:1) after heating for 2 h at 1523 K (1250 °C). In the case of the alumina mixture, barium aluminates ($BaAl_2O_4$) are the major phase formed as seen by the highest intensity of its peaks; alumina and unreacted barium sulphates are also present (Fig. 3a). In the case of silica, barium silicate is formed whilst peaks of residual quartz (initial form of silica) and barium sulphate are also seen (Fig. 3b). Weight loss calculations of the $BaSO_4/Al_2O_3$ and $BaSO_4/SiO_2$ mixtures indicated losses of 15 and 20%, respectively, which are attributed to the release of SO_2 and O_2 gases due to decomposition accompanying the reactions. This is supported by other studies which have shown that barium aluminate formation occurs through the reactions of Al_2O_3 with BaO (formed from $BaSO_4$ decomposition) even at temperatures close to 1373 K (1100 °C) [44]. Moreover, these results indicate that $BaSO_4$ decomposition is enhanced in the presence of alumina and silica.

Figure 4 shows the XRD pattern of the mixture of Al_2O_3, SiO_2 and $BaSO_4$ (1:1:2 wt%) after heat treatment for 2 h at 1523 K (1250 °C); this is to simulate the sum of the two ratios used previously. In this case, celsian is clearly the major reaction product. Celsian formation could occur through an overall reaction combining the decomposition step, as given by Eq. 2 [45].

$$BaSO_4 + Al_2O_3 + 2SiO_2 \rightarrow BaAl_2Si_2O_8 + SO_2 + {}^1/_2O_2 \quad (2)$$

Effect of $BaSO_4$ concentration on celsian formation after heat treatment

Figure 5a compares the XRD patterns of the refractory samples having varying $BaSO_4$ concentrations after heating at 1523 K (1250 °C), whilst Fig. 5b shows the magnified view of the critical peaks in the angular range (2θ) 20–30°. All the heated samples showed that the highest intensity peak to be of alumina (Al_2O_3), which was expected due to the high-alumina content in the refractory. It must also be noted that the alumina is present as the phase corundum (α-alumina). The XRD analysis of sample BR0 (not presented here) showed that in addition to alumina, some mullite is present [30].

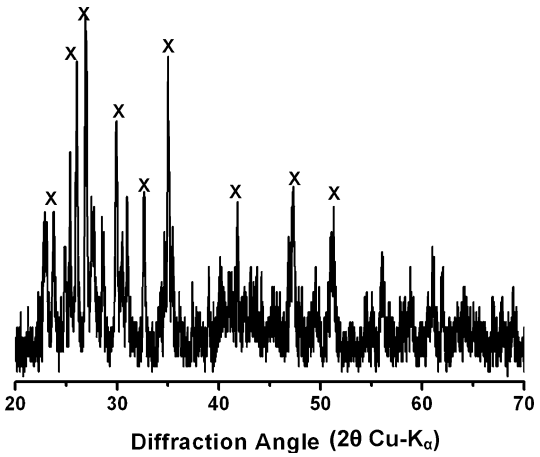

Fig. 4 XRD pattern of a mixture of Al_2O_3, SiO_2 and $BaSO_4$ in a ratio of 1:1:2 by weight after heat treatment at 1523 K (1250 °C) for 2 h in the absence of Al-alloy (X-Celsian)

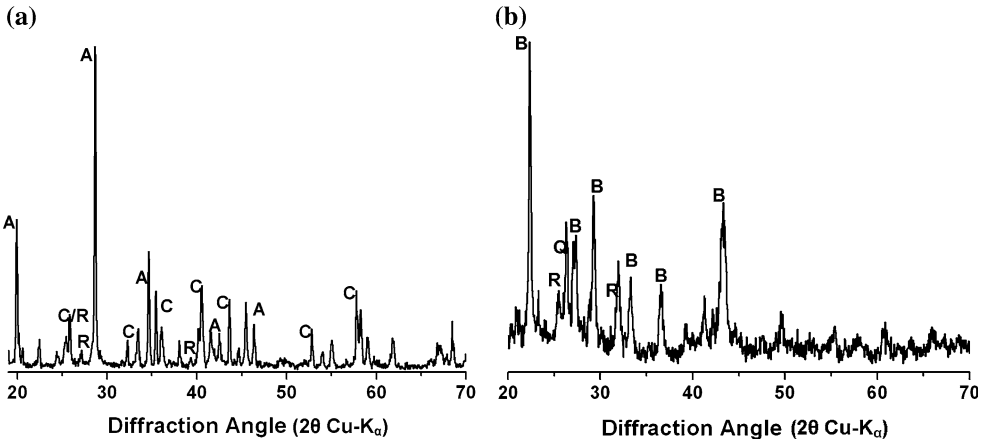

Fig. 3 XRD patterns of equal mixtures (by weight) of **a** Al_2O_3 and $BaSO_4$ and **b** SiO_2 and $BaSO_4$ after heat treatment at 1523 K (1250 °C) for 2 h in the absence of Al-alloy (A-Barium aluminate, C-Alumina, R-Barium Sulphate, B-Barium Silicate and Q-Quartz)

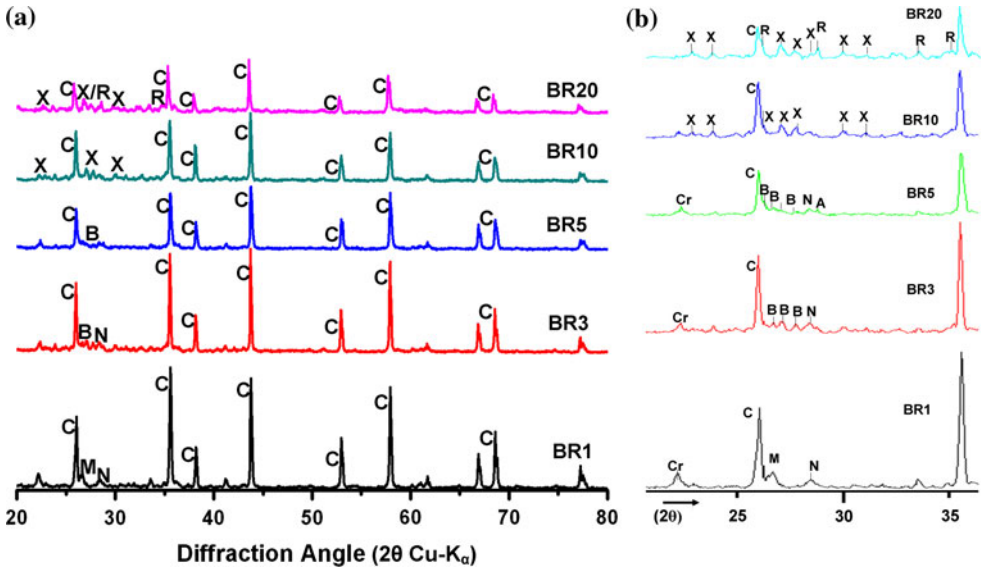

Fig. 5 Effect of heat treatment at 1523 K (1250 °C) for 2 h on refractories containing varying $BaSO_4$ contents in the absence of Al-alloy **a** major peaks in the angular range of 20–80° (diffraction angle 2θ Cu Kα) and **b** magnified view of peaks in the range 20–30° (N-Anorthite, R-barium sulphate, C-Alumina, M-Mullite, X-Celsian, B-Barium silicate and Cr-Cristobalite)

From the figure, in sample BR1, small peaks of mullite and anorthite can be seen in addition to the alumina peaks. Comparison of the XRD patterns of samples BR1, BR3 and BR5 showed that as $BaSO_4$ increases to 3 and 5 wt%, the intensity of mullite and anorthite peaks decreases such that they completely disappear in sample BR5. The change in these peaks was also accompanied by the simultaneous increase in the intensity of barium silicate peaks. In samples with $BaSO_4 \geq 10$ wt% (BR10 and BR20), barium occurs as barium aluminosilicate–celsian ($BaAl_2Si_2O_8$) rather than as barium silicate. The XRD pattern of sample BR20 also showed that barium sulphate peaks are present, implying that the barium sulphate was not completely consumed in the reactions with the other refractory constituents.

At low $BaSO_4$ concentrations (1 wt%), the cement phase, usually a combination of calcium aluminates ($CaAl_2O_4$) and calcium dialuminates ($CaAl_4O_7$), reacts with silica and mullite in the refractory to form anorthite. Under the tested conditions, thermodynamically (based on FACT-Sage calculations [46]) these reactions could occur as shown by Eqs. 3 and 4. The Gibbs free energy for these reactions was in the range from −70 to −85 kJ at 1523 K (1250 °C).

$$CaAl_4O_7 + 2SiO_2 \rightarrow CaAl_2Si_2O_8 + Al_2O_3 \quad (3)$$

$$CaAl_2O_4 + 2SiO_2 \rightarrow CaAl_2Si_2O_8 \quad (4)$$

With increasing addition of $BaSO_4$ (3–5 wt%) to the refractory, the anorthite content showed a corresponding decrease whilst the formation of barium silicates is enhanced. The increasing $BaSO_4$ content reacts with SiO_2 (quartz/microsilica) or mullite present in the refractory to form barium silicates. However, BR3 and BR5 samples indicated the presence of barium silicates without any barium aluminates. This could be attributed to the greater reactivity of amorphous microsilica present in the refractory compared to alumina [29] leading to increased chances for barium silicate formation in the refractory within the experimental time as compared to aluminates [29]. Furthermore, with increase in the $BaSO_4$ content ≥10 wt%, barium silicates start to react with alumina and silica in the refractory to form celsian. Our observation of celsian formation is consistent with a past study in which barium silicates were the precursor to celsian formation (Eq. 5) [32]. Moreover, these observations are consistent with those based on pure mixtures discussed earlier in "Thermal decomposition of $BaSO_4$ with silica and alumina" section.

$$Ba_2SiO_4 + 2Al_2O_3 + 3SiO_2 \rightarrow 2[BaAl_2Si_2O_8] \quad (5)$$

Interfacial behaviour of the Al-alloy/refractory system

For all the samples, the EPMA of the alloy droplets indicated complete loss of Zn from the alloy as is often the case in industrial conditions. The loss of Zn alloy decreases the viscosity, which would then increase the intensity of the interfacial reactions and associated metal penetration [47].

Effect of $BaSO_4$

A heat-treated pure $BaSO_4$ substrate was reacted with the Al-alloy at 1523 K (1250 °C) for 2 h. Figure 6a and b shows the interfacial region between the Al-alloy and the $BaSO_4$ substrate. Pores ranging in size from 50 to 200 μm can be seen in the substrate which confirms the loss of gaseous sulphur oxides as a consequence of $BaSO_4$ decomposition to BaO and SO_2. This is further substantiated through a lower than expected distribution of sulphur in the substrate as seen from the elemental mapping. The

loss of sulphur results in localised regions rich in barium oxides in the substrate (Fig. 6b).

Figure 6a further shows that the molten Al-alloy has penetrated to a depth of 100 μm in the $BaSO_4$ substrate, leaving a layer of barium aluminates at the interface. This shows that in the absence of silica and alumina, the reactions with the Al-alloy result in the formation of barium oxides and barium aluminates. In the refractories which contain Al_2O_3 and SiO_2 in addition to $BaSO_4$, the reactions would involve both in situ reactions between the refractory constituents as well as individual reactions with the Al-alloy.

Effect of anorthite and alumina

Figure 7a and b illustrates the typical Mg and Al maps, respectively, whilst Fig. 7c shows the combined mapping of Al and Mg elements illustrating their association. A similar system of combining the elemental maps is followed for all the other interfacial images.

In the absence of any additive, the elemental mapping of the interface between the refractory BR0 and the Al-alloy after reactions for 2 h at 1523 K (1250 °C) shows that alumina and Mg-spinel are the major phases in the system (Fig. 7c). After the completion of the test, a small portion of the refractory sample containing a Mg-spinel layer (of 50–80 μm thickness) was strongly attached to the alloy. The same figure further shows that the molten alloy penetrated to a depth of 150–200 μm from the interface. Mg is believed to initially vaporise and preferentially reduce the refractory oxides [24, 26], thereby making the refractory more prone to subsequent aluminium attack. The typical refractory discoloration associated with the initial reduction by Mg, which was clearly seen in other studies [24, 33, 34], was also observed in these samples. The reactions of the alloy constituents (Mg and Al) have been discussed in detail previously [34].

Figure 8b shows the interfacial region between the Al-alloy and the BR1 system after reactions for 2 h at 1523 K (1250 °C). From the figure, it is seen that the Mg from the alloy has penetrated into the refractory to an average depth of 200 μm, and the reaction has mainly occurred with the calcium aluminosilicate phases, rather than with the alumina grains. Mg reactions with anorthite would form Mg-spinel and magnesium calcium silicate ($MgO{\cdot}2CaO{\cdot}2SiO_2$—akermanite) which would be further reduced to merwinite or calcium aluminate phases by reactions with the Al-metal [34]. Moreover, these reactions would result in the diffusion of elemental Si into the molten alloy. Furthermore, Al reacts with anorthite to form calcium aluminosilicates and calcium aluminates, and the reactions with the aluminosilicates would cease with the formation of a thick interfacial penetrated layer, or once all the products have been reduced to Mg-spinel or calcium aluminates [33, 48].

Figure 8b further reveals that a refractory layer (50–70 μm thick) is bonded strongly to the Al-alloy, whilst a thin layer (<10 μm) is observed to line the interface between the alloy and the bonded refractory portion, which is seen to be comprising sulphur-rich species. This layer has formed due to the reactions of sulphur oxides released from the decomposition of $BaSO_4$ with the calcium cement phases present close to the interface, as they passed through the bulk refractory, leading to the formation of $CaSO_4$ at the interface. The localisation of the sulphur layer close to the interface indicates that the gases such as SO_2 cannot diffuse through the alloy easily and tend to be trapped at the interface. The continuity of this layer is believed to decrease further reactions/penetration of the alloy into the refractory.

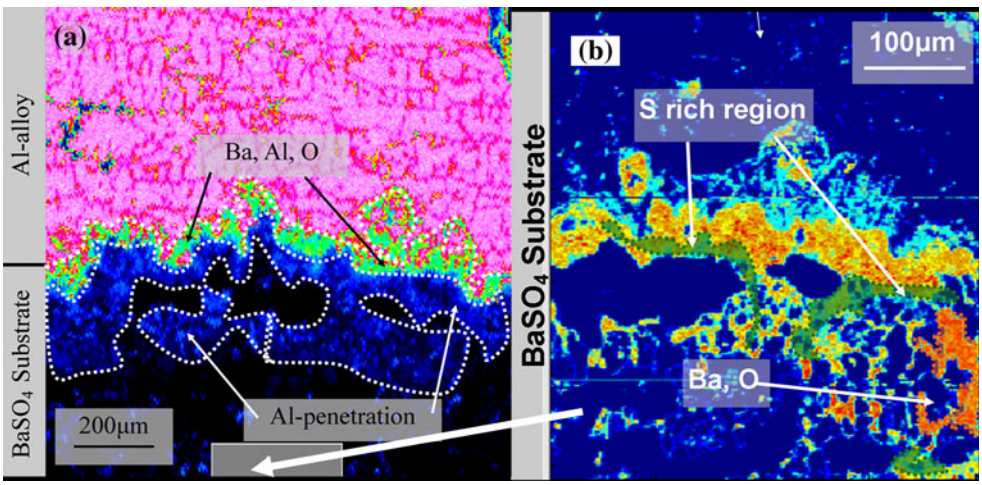

Fig. 6 Elemental mapping of the **a** interface and **b** interior region of the substrate (magnified image of the region shown in *inset* in **a**) for the Al-alloy/$BaSO_4$ system after reactions for 2 h at 1523 K (1250 °C) (Ba–O indicates barium oxide, Ba–Al–O indicates barium aluminates)

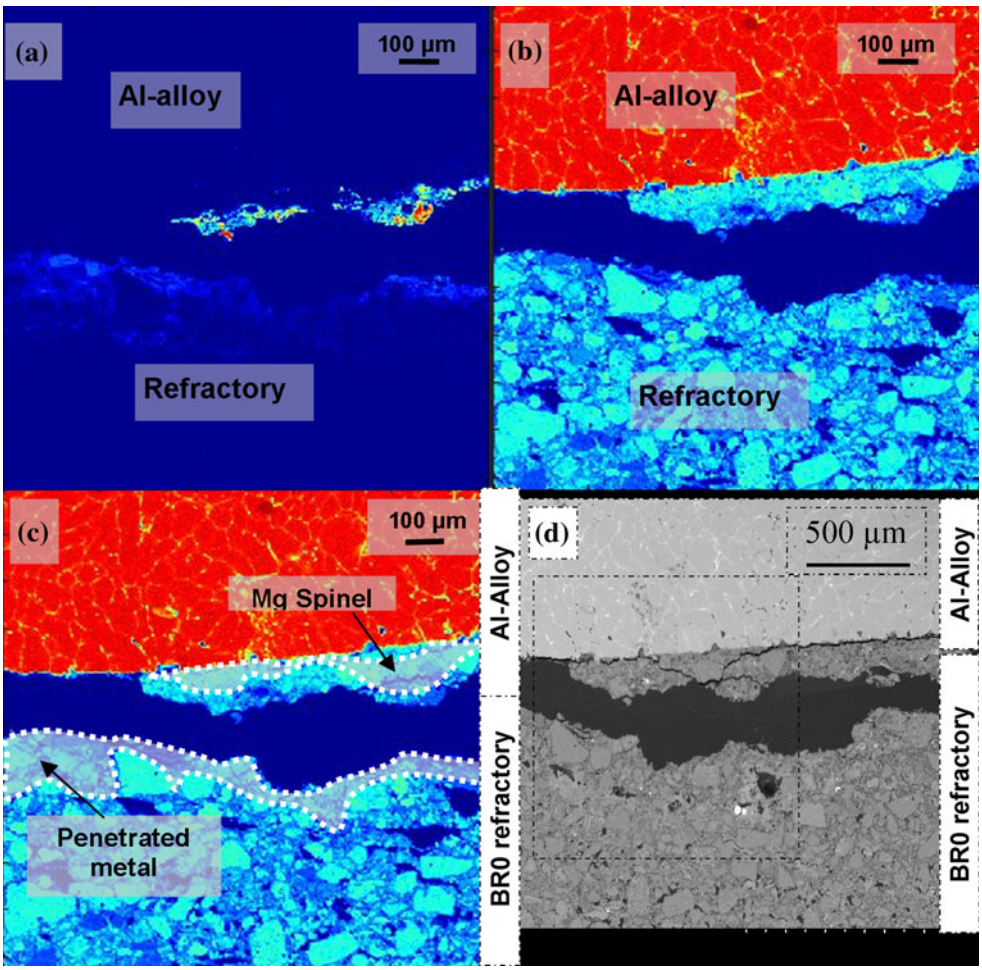

Fig. 7 Elemental mapping of the interface between Al-alloy and BR0 substrate after reactions at 1523 K (1250 °C) for 2 h, showing the distribution of **a** Mg, **b** Al and **c** Al map with Mg mapping superimposed. **d** BSE image (50×) of the interfacial region (rectangle shows the region considered for elemental maps)

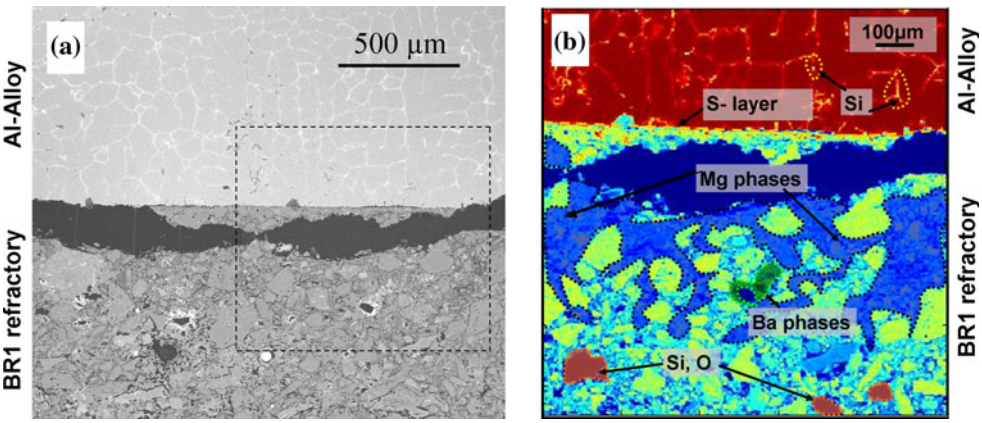

Fig. 8 **a** BSE image (50×) of the interfacial region (rectangle shows the region considered for the elemental mapping) and **b** elemental mapping of the Al-alloy/BR1 refractory substrate after reactions at 1523 K (1250 °C) for 2 h (Ba phases indicate primarily barium silicates, Si–O indicates silica and Mg phases indicate Mg-penetrated regions)

Effect of barium silicates

Figure 9b shows the interfacial changes in the Al-alloy/BR3 refractory system after reactions for 2 h at 1523 K (1250 °C). From the figure, it is observed that the Mg phases have penetrated into the refractory to a depth of almost 300 μm from the interface. Moreover, a thin (<10 μm) sulphur-rich interfacial layer is present between the alloy and the refractory, whilst barium-rich regions deficient of sulphur containing phases were present in the bulk refractory.

Figure 10b shows the BR5 refractory after reaction with the alloy for 2 h at 1523 K (1250 °C). From the figure, it is clear that the Mg penetration into the refractory was even more extensive (depth of more than 300 μm) than in the case of sample BR3. Furthermore, in both these samples,

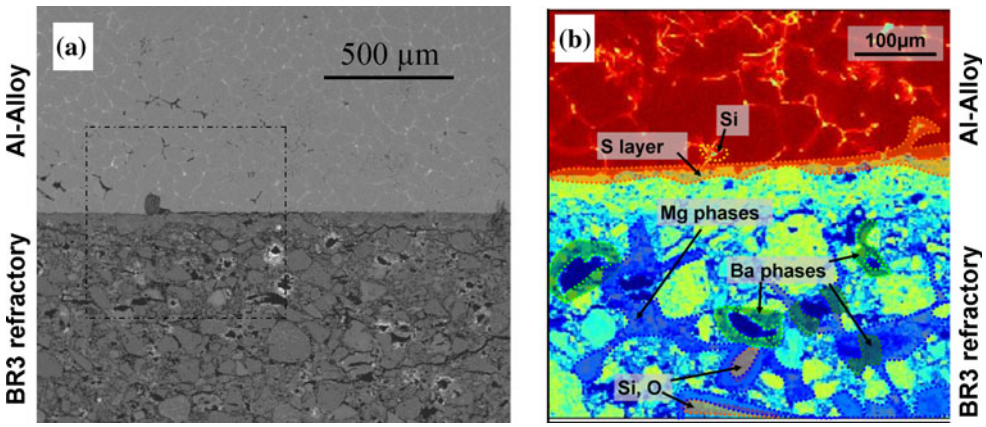

Fig. 9 **a** BSE image (50×) of the interfacial region (rectangle shows the region considered for the elemental mapping) and **b** elemental mapping of the interfacial region for the Al-alloy/BR3 refractory substrate after reactions at 1523 K (1250 °C) for 2 h (Ba phases indicate primarily barium silicates, Si–O indicates silica and Mg phases indicate Mg-penetrated regions)

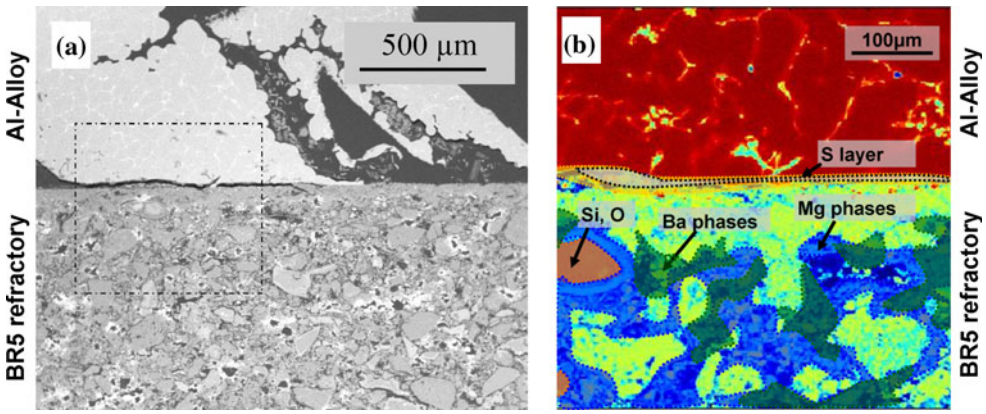

Fig. 10 **a** BSE image (50×) of the interfacial region (rectangle shows the region considered for the elemental mapping) and **b** elemental mapping of the interfacial region for the Al-alloy/BR5 refractory substrate after reactions at 1523 K (1250 °C) for 2 h (Ba phases indicate primarily barium silicates, Si–O indicates silica and Mg phases indicate Mg-penetrated regions)

barium phases were found to be present surrounding the Si-rich grains, and EPM analysis revealed them to be barium silicates. These phases formed at the grain boundaries are poorly crystalline and this explains their increased reactions with Mg from the alloy.

Similar to the previous systems, Mg vapour penetration is believed to initiate the interfacial reactions. Mg reacts with the barium silicates reducing them to elemental Si which is picked up by the alloy (Eq. 6). Further barium silicate reduction by aluminium metal occurs next, resulting in the formation of barium aluminates and elemental Si (Eq. 7). The formation of barium aluminates stops the reactions, as they are not reduced by the aluminium metal. The reduction of barium silicates in the refractory samples BR3 and BR5 is consistent with the extent of penetration observed in these samples. The Gibbs free energy values for these reactions were approximately −150 kJ at 1523 K (1250 °C) [46].

$$2[BaSiO_3] + 2Mg \rightarrow Ba_2SiO_4 + 2MgO + Si \quad (6)$$

$$3[Ba_2SiO_4] + 4Al \rightarrow 2[Ba_3Al_2O_6] + 3Si \quad (7)$$

Effect of celsian and unreacted $BaSO_4$

Figure 11b shows the elemental mapping for the interface between the refractory BR10 and the Al-alloy after reactions for 2 h at 1523 K (1250 °C), whilst Fig. 12b shows the interfacial mapping for the BR20/Al-alloy system after reactions for 2 h at 1523 K (1250 °C). Comparing Fig. 11b with Figs. 9b and 10b, it is clearly seen that the extent and continuity of Mg penetration into the refractory is considerably reduced (less than 100–150 µm) as compared to samples BR3 and BR5. Moreover, the refractory matrix is rich in barium-containing phases, which are believed to be either celsian or a product formed by celsian reactions with the Al-alloy. Even though some studies have suggested that celsian could be reduced by Al-alloy [49], the kinetics of the reaction are retarded by the formation of barium aluminates and alumina at the interface which would prevent further reactions of the refractory with the alloy.

From Fig. 12b, it is also observed that in sample BR20, there are even some regions where Ba and S phases are closely associated, indicating the presence of unreacted $BaSO_4$. This clearly confirms that the decomposition of barium sulphate is influenced by the relative presence of silica and alumina in the refractory, with the presence of silica believed to be more crucial owing to its greater ease of reactions with $BaSO_4$ due to its presence as amorphous microsilica. However, the increased presence of barium sulphate in the refractory would result in increased

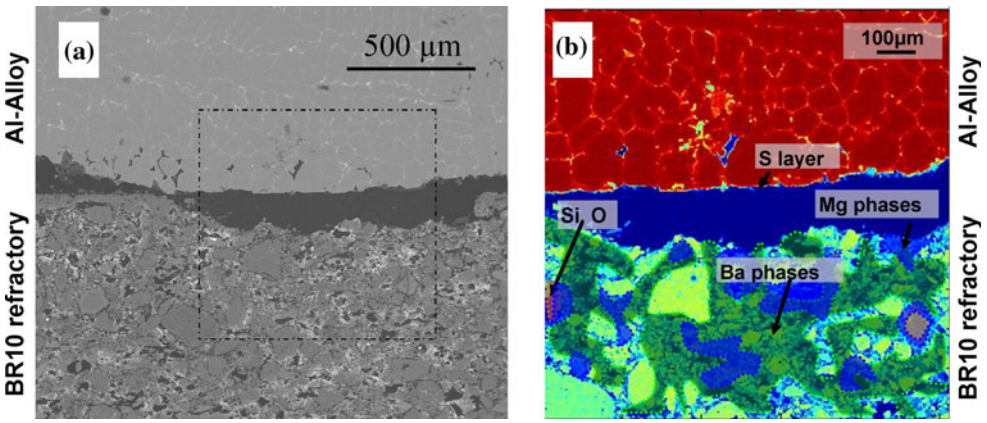

Fig. 11 **a** BSE image (50×) of the interfacial region (rectangle shows the region considered for the elemental mapping) and **b** elemental mapping of the interfacial region for the Al-alloy/BR10 refractory substrate after reactions at 1523 K (1250 °C) for 2 h (Ba phases indicate primarily celsian and Mg phases indicate Mg-penetrated regions)

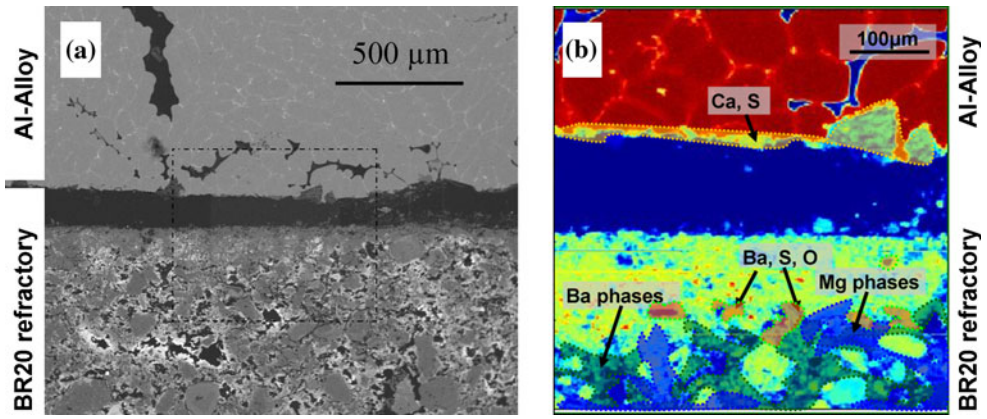

Fig. 12 **a** BSE image (50×) of the interfacial region (rectangle shows the region considered for the elemental mapping) and **b** elemental mapping of the interfacial regions for the Al-alloy/BR20 refractory sample after reactions at 1523 K (1250 °C) for 2 h (Ba phases indicate primarily celsian, Ba–S–O indicates unreacted barium sulphates and Mg phases indicate Mg-penetrated regions)

reactions with the alloy (as seen in "Effect of $BaSO_4$" section), leading to generation of volatiles, which would subsequently increase the porosity in the refractory, thereby enhancing the alloy penetration into the refractory. The porosity of the BR20 samples was estimated to be close to 30 vol%, which is higher than that observed for the other samples (15–20 vol%), and this explains the greater penetration observed in the former sample.

Table 3 summarises the average alloy penetration into the different refractory samples, and this can be considered to be an indicator of the refractory performance. The additive range of $BaSO_4$ used and its influence on refractory performance can be understood as follows.

At low concentrations ($\leq$1 wt%), the $BaSO_4$ amount is insignificant to have any effect on the refractory behaviour. At this concentration level, anorthite is the major species present in the refractory other than corundum, and their combined presence results in a slight improvement of the resistance to metal penetration. The positive effect of anorthite in improving the corrosion resistance was also seen in the case of high-alumina refractory samples containing CaF_2 (in 1–3 wt%) [34].

When $BaSO_4$ is in the range 3–5 wt%, barium silicate formation occurs due to reactions between $BaSO_4$ and silica-containing phases in the refractory. The barium silicates are glassy phases which undergo reactions with the Al-alloy and allow for greater metal penetration into the refractory. Also at these concentrations, the anorthite is too low to have any impact on the resistance to metal reactions and penetration. Samples containing CaF_2 in a similar range were observed to show much greater resistance to penetration due to the combined effect of the additive coupled with anorthite formation [34].

At higher concentration ranges (10 wt% and above), barium aluminosilicate–celsian is observed to form due to the reactions of barium silicates with excess alumina in the refractory. This results in an improvement in the corrosion resistance leading to the retardation of the alloy penetration into the refractory. Thus the optimum level with regard to barium sulphate addition to high-alumina refractories has been determined to be 10 wt% in this study. From a previous study focusing on CaF_2 addition, the optimum content was determined to be <5 wt% since above this level,

Table 3 Average alloy penetration into the refractory samples

Sample	BR0	BR1	BR3	BR5	BR10	BR20
Average penetration depth (µm)	~200	~170	>300	>300	~125	~170

glassy phases consisting of anorthite matrix with CaF_2 crystallites were formed which enhanced reactions with the alloy leading to extensive alloy penetration [34].

Conclusions

A study of the interfacial behaviour of Al-alloy with a high-alumina refractory was carried out to investigate the effect of $BaSO_4$ contents in the refractory on the interfacial reactions at 1523 K (1250 °C). The following conclusions were made:

- This study showed that barium sulphate decomposes at the experimental temperatures in the presence of alumina, and silica and this was the initial step leading to the formation of barium aluminates, silicates or aluminosilicates depending on the relative concentrations of the initial species.
- Barium sulphate reacts with molten Al-alloy resulting in the formation of barium aluminates at the interface. Sulphur dioxides are released during the decomposition at this temperature, and this would result in the formation of a highly porous matrix containing barium oxides.
- In all the samples tested at 1523 K (1250 °C), alumina was the dominant interfacial product as expected. In the absence of any additive, the reactions between the refractory and the Al-alloy led to the formation of alumina and Mg-spinel phases close to the interface.
- At 1 wt%, $BaSO_4$, anorthite was also formed due to the reactions of the calcium cement phases with the refractory constituents. However, with the increase in the $BaSO_4$ content to 5 wt%, barium silicate formation occurred at the expense of anorthite. Samples with $BaSO_4$ contents between 3 and 5 wt% reacted strongly with the alloy, with extensive penetration of Mg from the alloy into the refractory (>300 μm), and the reduction of barium silicate phases. However, the presence of these glassy barium silicate phases prevented the Mg phases from penetrating to further depths into the refractory, and also prevented Mg reactions with alumina to form spinel.
- Further increase in the additive content to 10 wt% and more resulted in the formation of celsian, which caused a decrease in the intensity of reactions with Al-alloy, owing to its role in lowering the free silica available for reaction with the alloy. This resulted in a decrease in the alloy penetration (<150 μm) into the refractory in these samples.
- However, samples which contained higher $BaSO_4$ contents (20 wt%) showed greater penetration of the alloy (~170 μm). This is attributed to the presence of unreacted excess $BaSO_4$ which would be reduced by the alloy leading to increased porosity formation due to the loss of SO_2 during the reactions.

References

1. Sustainability Report (2006) Australian Aluminium Council. www.aluminium.org.au
2. Hemrick JG, Headrick WL, Peters K-M (2008) Int J Appl Ceram Technol 5(3):265
3. Allaire C, Guermazi M (2000) In: Peterson RD (ed) Proceedings of light metals. The Minerals, Metals & Materials Society (TMS), pp 685–691
4. Choate WT, Green JAS (2003) US energy requirements for aluminum production: historical perspective, theoretical limits and new opportunities. Prepared for the US Department of Energy - Energy Efficiency and Renewable Energy, Washington, DC
5. Brondyke KJ (1953) J Am Ceram Soc 36(5):171
6. U.S. Energy Requirements for Aluminium Production (February 2003) U.S. Department of Energy, Washington DC. Prepared for the Energy Efficiency and Renewable Energy Industrial Technologies Program
7. Pauline M, Turner S (1999) In: White P, Grandfiel J (eds) 6th Australian, Asia Pacific conference. TMS, USA, pp 77–83
8. Lee W, Moore R (1998) J Am Ceram Soc 81(6):1385
9. Champion J, Keene B, Sillwood J (1969) J Mater Sci 4:39. doi: 10.1007/BF00555046
10. Ksiazek M, Sobczak N, Mikulowski B, Radziwill W, Surowiak I (2002) Mater Sci Eng 324A:162
11. Levi G, Kaplan WD (2002) Acta Mater 50(1):75
12. Levi G, Kaplan WD (2003) Acta Mater 51(10):2793
13. Saiz E, Tomsia A, Suganuma K (2003) J Eur Ceram Soc 23:2787
14. Sobczak N, Asthana R, Ksiazek M, Radziwill W, Mikulowski B (2004) Metall Mater Trans A 35(3):911
15. Asthana R, Sobczak N (Jan 2000) JOM-e: overview. TMS
16. Zhou X, De Hosson JThM (1996) Acta Mater 44(2):421
17. Mortensen A, Drevet B, Eustathopoulos N (1997) Scripta Mater 36(6):645
18. Eustathopoulos N, Sobczak N, Passerone A, Nogi K (2005) J Mater Sci 40:2271. doi:10.1007/s10853-005-1945-4
19. Lee WE, Zhang S (2000) In: Oprea G (ed) Proceedings of the 9th symposium on refractories for the aluminium industry. Refractories for the next millennium. The Minerals, Metals and Materials Society (TMS), pp 177–187
20. Ownby P, Li KWK, Weirauch DA Jr (1991) J Am Ceram Soc 74(6):75
21. Siljan O-J, Schoning C (2002) Refract Appl News 8(1):21
22. Siljan O-J, Rian G, Pettersen DT, Solheim A, Schoning CR (2002) Refract Appl News 7(6):17
23. Afshar S, Allaire C (2000) JOM 52(5):43
24. Afshar S, Allaire C (2001) JOM 53(8):24
25. Allahevrdi M, Afshar S, Allaire C (1998) JOM 50(2):30
26. Afshar S, Allaire C (1996) JOM 48(5):23
27. Afshar S, Gaubert C, Allaire C (2003) JOM 55(4):66
28. Pereira PFA, Baldo JB (1997) In: Proceedings of the unified international technical conference on refractories—UNITECR' 97, New Orleans, LA. American Ceramic Society, Westerville, OH, pp 1667–1676
29. Koshy P (2009) Effect of chemical additives on the interfacial phenomena of high alumina refractories with Al-alloys. PhD thesis, UNSW, Australia

30. Gupta S, Koshy P, Sahajwalla V, Pauline M, Leicht N (2005) UNITECR 05, Orlando, FL, USA. ACS, pp 630–634
31. Chakraborty AK (2003) Thermochim Acta 398(1–2):203
32. Schmutzler HJ, Sandhage KH (1995) Metall Mater Trans B 26:135
33. Koshy P, Gupta S, Sahajwalla V, Edwards P (2008) Metall Mater Trans B 39(2):331
34. Koshy P, Gupta S, Sahajwalla V, Edwards P (2008) Metall Mater Trans B 39(4):603
35. Kapilashrami E, Jakobsson A, Lahiri AK, Seetharaman S (2003) Metall Mater Trans B 34(2):193
36. Kapilashrami E, Lahiri AK, Cramb AW, Seetharaman S (2003) Metall Mater Trans B 34(5):647
37. Zhao L, Sahajwalla V (2003) ISIJ Int 43(1):1
38. Rocha-Rangel E, Becher P, Lara-Curzio E (2003) Mater Sci Forum 442:97
39. Fujii H, Nakae H, Okada K (1993) Metall Mater Trans B 24:1391
40. Laurent V, Chatain D, Chatillon C, Eustathopoulos N (1988) Acta Metall 36:1797
41. Stern KH (2000) High temperature properties and thermal decomposition of inorganic salts with oxyanions. CRC Press, p 78
42. Mohazzabi P, Searchy AW (1976) J Chem Soc 411:291
43. Lide DR (2003) Handbook of chemistry and physics, 84th edn. CRC Press, Cleveland, OH, p 129
44. L'vov BV, Ugolkov VL (2004) Thermochim Acta 411(1):73
45. Maslennikova GN, Fomina NP, Kharitonov FY, Naidenova GA (1974) Glass Ceram 31(12):872
46. FactSage 6.0, GTT Technologies, Germany (2009)
47. Furness G, Forde A (1999) Light metals 128th TMS annual meeting, San Diego USA, pp 975–993
48. Buchel G, Buhr A, Gierisch D, Racher RP (2005) In: Smith J (ed) Proceedings of UNITECR'05, Orlando, USA. ACS, pp 462–467
49. Oliveira M, Agathopoulos S, Ferreira JMF (2002) Acta Mater 50:1441